Low Temperature Physics/Fizika Nizkikh Temperatur, 2020, vol. 46, No. 12, pp. 1386–1393

Low-temperature luminescence of catangasite single crystals under excitation by vacuum ultraviolet synchrotron radiation

A. P. Kozlova[1], O. A. Buzanov[2], V. Pankratova[3], and V. Pankratov[3]

[1]*National University of Science and Technology «MISiS», Moscow 119049, Russia*
E-mail: kozlova.ap@misis.ru

[2]*JSC Fomos-Materials, Moscow 107023, Russia*

[3]*Institute of Solid State Physics, University of Latvia, Riga LV-1063, Latvia*

Received July 24, 2020, published online October 21, 2020

The luminescent properties of $Ca_3TaGa_3Si_2O_{14}$ (CTGS, catangasite) single crystals have been studied by means of the vacuum ultraviolet excitation spectroscopy utilizing synchrotron radiation from 1.5 GeV storage ring of MAX IV synchrotron facility. Two emission bands at 320 nm (3.87 eV) and 445 nm (2.78 eV) have been detected. Examining excitation spectra in vacuum ultraviolet spectral range, the 320 nm emission band was explained as the emission band of self-trapped exciton in CTGS single crystal. Its atomic structure is discussed. It is also proposed that the 445 nm (2.78 eV) emission in the CTGS is due to the *F* centers, which have shown a well-resolved excitation (absorption) band at 5.1 eV (243 nm).

Keywords: catangasite, langasite, langatate, VUV luminescence spectroscopy, synchrotron radiation.

Introduction

Crystals with Ca-gallogermanate structure ($Ca_3Ga_2Ge_4O_{14}$) are known and have been studied for about forty years [1]. Moreover, according to the literature data and the number of scientific teams investigating these materials, interest in this crystals family is strongly increasing so far. Some of the most famous representatives are $La_3Ga_5SiO_{14}$ (LGS, langasite), $La_3Ga_{5,5}Ta_{0,5}O_{14}$ (LGT, langatate) and $Ca_3TaGa_3Si_2O_{14}$ (CTGS, catangasite).

The structure of these crystals belongs to the space group of symmetry of P_{321} consistent with the crystal class 32 to which quartz also belongs. According to ionic distribution, langasite and langatate are disordered compounds, while catangasite is an ordered one [2–5]. In ordered crystals all the positions of the same type are occupied by one type of ions, in disordered one type of position is statistically occupied by two types of atoms. The characteristic feature of Ca-gallogermanate structure is the presence of two layers, which are perpendicular to the threefold axis [5]. The decahedral positions occupied by La^{3+} in LGS and LGT and Ca^{2+} in CTGS and octahedral positions occupied by Ga^{3+}/Ta^{5+} in LGT, Ga^{3+} in LGS and Ta^{5+} in CTGS form one layer. Another layer consists of two types of tetrahedral positions: they are entirely occupied by Ga^{3+} in LGT. In the case of LGS one of these positions is shared between Si^{4+} and Ga^{3+}, in another one Ga^{3+} is placed. Ga^{3+} also occupies the same position in GTGS, while Si^{4+} is located in another tetrahedral position. Thereby, the position with partial substitution of two types of ions leads to a certain structural disorder [6].

LGS, LGT and CTGS crystals can be grown by different methods: the floating zone method [7], micro-pulling-down method [8], the Bridgman method [9, 10] and the Czochralski method [11–14], which is the most widespread among others. Moreover, the growth atmosphere significantly affects the quality and properties of these crystals. The strong deviation from stoichiometry is observed in crystals grown in protective atmosphere of pure argon or nitrogen due to gallium suboxide evaporation. In order to suppress such deviation some amount of oxygen should be added to the growth atmosphere. Crystals grown in various atmospheres differ in color and size: in atmosphere of argon with oxygen as-grown crystals are colored from light yellow (in case of CTGS) to rich orange (in case of LGS and LGT) and a larger size, while crystals obtained in the pure argon are colorless [2, 15, 16].

In modern science and technology, these compounds are listed among the functional synthetic crystals found their application due to their superior laser, piezoelectric, and electro-optic (EO) properties [17, 18]. An attempt to use the LGS compound in a Pockels cell had not met with success until a Pockels cell with the quarter-wave configuration was used, leading to the self-compensation of the optical activity which crystals of this family possesses [17, 18]. This circumstance allows to consider LGS as a material suitable for fabricating cells for electro-optic laser *Q*-switching based on the rotation of polarized light due to electro-optic effects, including the linear Pockels effect [17, 19]. According to [20, 21] rare-earth containing LGT and especially LGS seem attractive for application in high-voltage optical sensors due to permitted longitudinal EO effect for anisotropic propagation directions along the twofold crystallographic axes, weak temperature dependence of this effect, and reasonably high EO coefficients. It is worth noting rare-earth free CTGS demonstrates strong temperature dependence of EO effect and relatively low electro-optic coefficients that does not allow to consider it for electro-optic voltage sensors for ac power lines. CTGS, LGT, LGS crystals are gyrotropic or optically active — light polarization plane $\rho_{\|}$ is rotated along the optical axis coinciding with the crystallographic threefold axis [2, 22, 23].

Development of sensors working at high temperatures and using the surface acoustic waves (SAW) technology requires the high temperature stability of piezoelectric coefficients and the presence of thermostable cuts from material which are observed in LGS and CTGS piezoelectric substrates [24, 25]. LGS, LGT and CGTS are used for filters with large pass bandwidths and resonators on the surface and bulk acoustic waves [4, 5, 26–28]. Such sensitive elements are required in aircraft turbine control systems, vehicle internal combustion engines, gas generators, vibration monitoring systems [29]. In several works [30, 31] the application of LGS as piezoelectric biosensors is described: the total frequency of a crystal is related to mass of crystal and the coated bioelement. The analyte binding or biochemical reaction results in resonant frequency, by measuring the variation in resonant frequency the analyzed concentration is detected. Some of biosensors are built with the SAW sensor and the shear-horizontal surface acoustic wave (SH-SAW) sensor based on langasite [31].

It was shown [32] that on the surface of the polar *X*-cut (110) of a piezoelectric $La_3Ga_{5,5}Ta_{0,5}O_{14}$ crystal a few layer graphene film was grown by the CVD method. This work implies that LGT substrates have the advanced catalytic ability in terms of catalyzing graphene formation in comparison with other dielectrics such as SiO_2 and sapphire. It was mentioned that the direct synthesis of few layer graphene on piezoelectric crystals of the langasite family provides the application of high-quality graphene in the fabrication of interdigital transducer structures for exciting the surface acoustic waves, in opto- and acousto-electronics as electrode structures, as well as in transparent conductive coatings to modulate and control optical radiation in crystals in solar cells and microsystems technology [32].

Furthermore, the numerous papers have dealt with the possible application of langasite family compounds as host for up-conversion pumped lasers, light-emitting LED phosphors [2, 3, 6, 13, 33–49]. Part of this research devoted to some spectroscopic features and luminescence performance of rare-earth doped (Eu^{3+}, Dy^{3+}, Er^{3+}, Ho^{3+}, Sm^{3+}, Fe^{3+}, Yb^{3+}+Er^{3+}, Nd^{3+}, Pr^{3+}, Ho^{3+}+Yb^{3+}) crystals is ascribed in [2, 3, 6, 13, 33–49]. On the other hand, intrinsic luminescence was detected and investigated in LGS, LGT and CTGS. Data on the intrinsic luminescence, as well as the absorption characteristics of the considered compounds are collected in Table 1.

It is worth noting that the linear dichroism phenomenon is observed in these crystals in the directions perpendicular to the optical axis [2, 3, 15, 36]. This means that the sample orientation during measurement considerably affects the optical spectra, in particular, the intensity of the measured optical parameters. However, the positions of the peaks of the absorption and luminescence spectra bands almost coincide regardless of the polarization of the propagating light or the orientation of the sample [6, 46].

Table 1 shows that intrinsic luminescence properties of CTGS are much less investigated comparing with both LGS and LGT compounds. Therefore, the main goal of current research is the study of intrinsic luminescence of CTGS single crystal. Taking into account that CTGS belongs to the class of wide band gap materials synchrotron radiation in vacuum ultraviolet (VUV) spectral range has been utilized. The luminescence spectroscopy under synchrotron radiation excitations was frequently applied in research of many wide band gap compounds including complex oxides [51–58], fluorides [59–62], iodides [62–64], chlorides [62, 65] and bromides [62, 66]. Moreover, synchrotron radiation was successfully utilized for luminescence studies of nanocrystalline semiconductors [67–69]. In this work we will demonstrate intrinsic luminescence and VUV excitation spectroscopy results obtained at the new synchrotron facility at MAX IV Laboratory for CTGS single crystals.

Experimental

Growth details

CTGS crystals were grown by the JSC FOMOS-Materials. The charge was produced in two stages by solid-phase synthesis. High purity (4N) $CaCO_3$, Ta_2O_5, Ga_2O_3, and SiO_2 powders were used as starting materials for charge. Pre-calcination of the starting materials was followed by weighing using the stoichiometric formula $Ca_3TaGa_3Si_2O_{14}$. The homogenization of this mixture was carried out in a vibrating unit with a liquid layer for 4 h. After the synthesis during 8h in a high-temperature furnace (Carbolite 16/35) at the temperature of 1150 °C, the next stage was the formation of high density tablets from the synthesized powder

Table 1. Absorption band and luminescence properties of LGS, LGT, and CTGS according to the literature

Crystal	Structure type	Band gap, eV	Luminescence					Absorption band, nm
			Excitation band	Emission band, nm	Experiment T, K	Possible luminescence center	Reference	
$La_3Ga_5SiO_{14}$ (LGS)	disordered	5.1 [36]	LGS (Ar)					235 (8 K) [46]
			8 eV	430	15	Interband electronic transitions	[36]	280 [36]
			210 nm	430	6	Intrinsic emission of excitons self-trapped on the GaO_6 complexes		340 [36]
			250 nm	470, 510		Antisite defects Si_{Ga}^{+} or Ga_{Si}^{-}		370 [36]
			220 nm	420	5	Self–trapped exciton luminescence	[46]	480 [36]
			245 nm	500		Radiative transition in lattice imperfection		1850 [36]
			LGS (Ar + O_2)					
			8 eV	460, 530	15	Defects in crystal structure	[36]	
			210 nm	430	6	Intrinsic emission of excitons self-trapped on the GaO_6 complexes		
			250 nm	470		Antisite defects Si_{Ga}^{+} or Ga_{Si}^{-}		
				530		Addition of oxygen in growth atmosphere/F centers (V_O^{2+}, $2e^{-}$)		
			205 nm	310	300	Self-trapped or trapped exciton emission	[47]	
			280 nm	370				
			260 nm	480		Defect-based origin proposed F^{+} centers		
$La_3Ga_{5.5}Ta_{0.5}O_{14}$ (LGT)	disordered	5.6 [33]	LGT (Ar)					242 (8 K) [46]
			x ray	430	300	Antisite defects $Ta_{Ga(2)}$	[33]	255 (80 K) [33]
			5.15 eV	410		Excitons trapped near antisite defects		290 (300 K) [33]
			4.75 eV	440		F centers in oxide		360 (300 K) [33]
			5.6 eV	440–450		Intrinsic emission excitons self-trapped at the TaO_6 molecular complexes		480 (300 K) [33]
			355 nm	428, 471,534	300	Exciton structure of luminescence centers	[35]	
				386, 402, 421, 449, 489,541	95	–		
			LGT (Ar+O_2)					
			x ray	430 560	300	Antisite defects $Ta_{Ga(2)}$	[33]	
			4.42 eV	410		Excitons trapped near antisite defects		
			5.6 eV	440		Emission of F centers		
				440–450		Intrinsic emission of excitons self-trapped at the TaO_6 molecular complexes		
			280 nm	550	4.2	Oxygen deficient oxyanionic molecular complexes, probably TaO_5 complexes		
			355 nm	414, 444, 487	300	Exciton structure of luminescence centers	[35]	
				414, 431, 451, 492, 589	95	–		
			< 225 nm	410	5	Radiative annihilation of self-trapped excitons	[46]	
			240 nm	460				
$Ca_3TaGa_3Si_2O_{14}$ (CTGS)	ordered	4.96 [50]	CTGS (Ar+O_2)					290 [2]
			x ray irradiation	340	300	Self-trapped excition (or defect luminescence; Charge transfer from octahedrally coordinated $[TaO_5]^{7-}$	[48]	360 [2]
		6.26	5.7 eV (excitonic peak)	320	10	Emission band of self-trapped exciton	[this work]	450 [2]
			5.1 eV	445		Emission of F/F^{+} centers		470–480 [2]
								610 [2]
								1790 [2]

by pressing at a force of up to 100 kN. The quantitative phase analysis by x ray diffraction was used to determine the completeness of the process. The main phase CTGS was 78 % of the initial mass, and the phase $Ca_4Ga_4Ta_2O_{15}$ was 22 %.

CTGS crystals were grown by the Czochralski method with the induction heating. A cylindrical iridium crucible with a diameter equal to its height was used for crystal growth and the growth atmosphere was mixture of the protective atmosphere of argon with the addition of 0.5–3 vol % oxygen.

Seed crystals were oriented along the [010] crystallographic axis. During the crystal growth the seed rotation rates and the crystal pulling rates were controlled to be 15–40 rpm and 0.5–1mm/h, respectively. The as-grown crystals were annealed at 1200 °C during 48 h. The as-grown crystals were transparent and yellowish.

Luminescence setup

The nominally undoped CTGS single crystal has been studied by means of luminescence spectroscopy technique under VUV excitations utilizing synchrotron radiation from 1.5 GeV storage ring of MAX IV synchrotron facility (Lund, Sweden). The experiments have been carried out on the photoluminescence endstation FINESTLUMI [70, 71] of the FinEstBeAMS undulator beamline [72]. The grazing incident monochromator of SX700 type (FMB Feinwerkind Messtechnik GmbH, Berlin) was applied for the monochromotization of synchrotron light. It contains the internally cooled plane mirror (M2) and two side-cooled plane gratings (PG1, 600 l/mm and PG2, 92 l/mm) intended for high and low energy ranges from 15 to 1500 eV and from 4.5 to 60 eV, respectively. In the current research, the PG2 mirror was utilized for the experiments under VUV excitations. The photon flux measured at a certain resolving power (R = 5000) was obtained of the order of 10^{13} ph/s. This value does not take into account the filters reducing the higher order of radiation. In order to suppress high orders of excitation a set of filters has been chosen. The quartz and MgF_2 filters were applied for 4.5–10.8 eV energy region. The excitation spectra were normalized utilizing the calibration curve obtained by means of AXUV-100G diode.

The Andor Shamrock (330i) spectrometer (0.3m) equipped with three gratings (300 l/mm, 300 nm blaze, 300 l/mm, 500 nm blaze, 1200 l/mm, 300 nm blaze) covers the spectral range 200–1500 nm. In the current research, the first grating was utilized for experiments. The Andor Shamrock spectrometer is an external spectrometer and a luminescence signal is delivered to the spectrometer by means of the optical fiber. Such registration method is especially successful in case of weak luminescence signal because it allows to collect efficiently emitted photons from the samples. The exit port of the Andor Shamrock spectrometer was equipped by the Hamamatsu (H8259-01) photomultiplier covering spectral range from 200 to 700 nm. The single crystals were installed on the cold finger of the cryostat placed in the high vacuum chamber (10^{-9} mbar). The close-cycle helium cryogenic system equipped with ARS-4HW compressor (Advanced Research System) and Lake Shore temperature controller provide sample temperature of 10 K.

Results and Discussion

Figure 1 exhibits luminescence spectra observed in the CTGS single crystal at 10 K under different excitation energies in VUV spectral range. It is clearly seen that each spectrum in Fig. 1 comprises at least two broad overlapped emission bands. The first one is responsible for a high-energy shoulder in the emission spectra peaking at about 320 nm. The second long wavelength band is the more intensive band. This emission band's spectral position can be estimated as 445 nm considering the emission spectrum under 5.1 eV excitation. Under other excitation energies, the high-energy emission band gives a contribution to the emission spectra slightly shifting the main emission peak towards high-energy side. On the other hand, the main emission peak could be not a single emission band but it results from the overlapping of two spectrally close bands. Therefore, the excitation spectra have been measured for three different emission wavelength marked by arrows in Fig. 1.

The excitation spectra for 320, 400, and 520 nm are depicted in Fig. 2 for the spectral range from 4.5 to 11 eV. The excitation spectra for two last emissions are similar. The only difference between them is the intensity of the excitation band at 5.1 eV.

On the other hand, the excitation spectrum at 320 nm does not reveal the excitation band at 5.1 eV at all. The excitation spectrum of the 320 nm emission has also another peculiarity that is absent in other excitation spectra, i. e. the sharp excitation peak at 5.7 eV, which can be explained as excitonic peak. The absorption coefficient in the

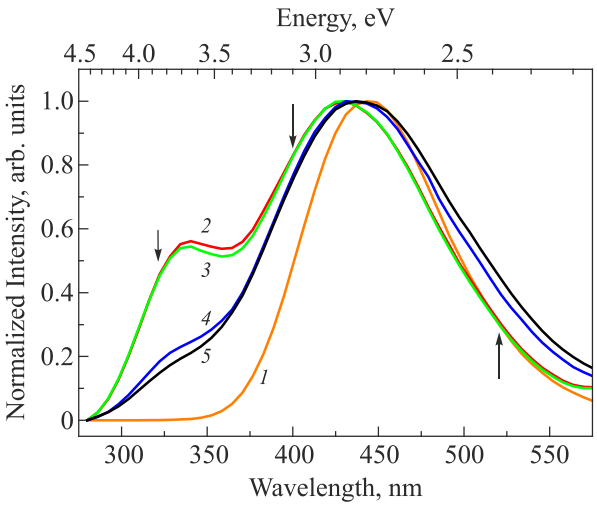

Fig. 1. (Color online) Luminescence spectra of CTGS single crystal under different excitations, eV: 5.1 (*1*), 5.7 (*2*), 6.5 (*3*), 8.0 (*4*), and 45 (*5*). T = 10 K.

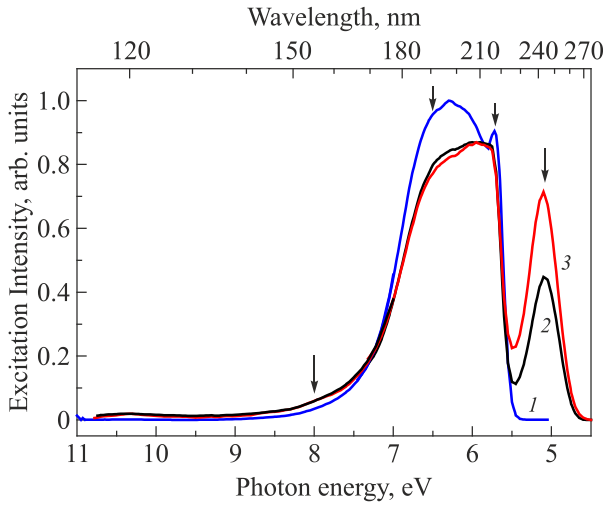

Fig. 2. (Color online) Excitation spectra in CTGS single crystal at T = 10 K monitoring 320 (*1*), 400 (*2*), and 520 (*3*) nm emissions. The arrows show the excitation energies that were utilized for the emission spectra recording in Fig. 1.

excitonic absorption peak is huge and, therefore, the intensity dip at 5.8 eV band is observed in the excitation spectrum of 320 nm emission. This energy can be considered as excitonic absorption energy in CTGS. Using the empirical equation $E_g = 1.08E_{ex}$ (where E_g is band gap energy, while E_{ex} is excitonic absorption energy) we can estimate the band gap energy value in CTGS as E_g = 6.26 eV. This value unexpectedly much higher than the value 4.96 eV reported before in literature [50]. We suggest that the excitation peak at about 5.1 eV was erroneously considered as excitonic one in [50].

Based on the excitation spectra in Fig. 2 we can conclude that the 5.1 eV band is located significantly lower than the band-to-band transitions in CTGS and, therefore, this excitation band relates to some defect or extrinsic center in CTGS single crystal. Next, the 320 nm emission band (Fig. 1) is absent in the emission spectrum under 5.1 eV excitation. Thus, this emission can be considered as intrinsic emission. Furthermore, we suggest that the 320 nm emission band is result of radiative recombination of self-trapped exciton (STE) in CTGS single crystal. Similar emission was observed before in [48] under x ray excitations at room temperature and the emission band was also suggested to be due to STE recombination. By analogy with LGT single crystals, we suggest that the STE in CTGS is localized within TaO_5 anion complex. Localization of STE in anion complex is typical for many complex oxides for instance tungstates [73–75], vanadates [53, 73], molibdates [73, 76], niobates [77–80] and titanates [81].

In contrast to the intrinsic emission at 320 nm (3.87 eV) the emission band at 445 nm (2.78 eV) most likely belongs to defect or extrinsic center. We suppose that the 5.1 eV (243 nm) excitation band and the corresponding 445 nm (2.78 eV) emission bands are excitation and emission bands of *F*-type center in CTGS. *F*-type center in many binary or complex oxides means oxygen vacancy which captures one or two electrons forming F^+ or F center, respectively [82]. Our suggestion about the origin of the 445 nm (2.78 eV) emission band in CTGS crystals is based on the analogy with LGS and LGT crystals. Taking into account the literature data (Table 1) the spectral positions of the excitation bands of F centers in LGS and LGT are 4.9 eV (253 nm) and 4.75 eV (261 nm), respectively, while emission bands are at 2.34 eV (530 nm) and 2.82 eV (440 nm) in LGS and LGT correspondingly. All these values are very close to the spectral characteristics of *F*-type centers obtained for the CTGS.

Luminescence intensities of both emissions (STE and F centers) are significantly decreasing if excitation energies become higher than 6.5 eV (Fig. 2). Moreover, luminescence excitation spectra exhibit negligible small luminescence intensities at excitation energies higher than 8 eV. Under high-energy excitations exceeding band gap energy value, electrons in the conduction band and holes in the valence band are created. If excitation energy is slightly higher than the band-gap value, charge carriers are not spatially separated over the crystal remaining within TaO_5 anion complex and subsequently forming STE after some relaxation. On the other hand, if excitation energy is much higher than the band gap, charge carriers will be distributed at long distance from each other relaxing separately without creation of STE. This explains the observed features in the excitation spectra depicted in Fig. 2.

Conclusions

Photoluminescence and excitation spectra of the catangasite single crystals have been measured under VUV excitations utilizing undulator synchrotron radiation from 1.5 GeV storage ring of MAX IV synchrotron. The emission peak at 320 nm is attributed to self-trapped excitons. The self-trapped excitons are effectively created within TaO_5 anion complex under the excitation energy slightly exceeding the band gap. Furthermore, the band gap of catangasite single crystal obtained from the excitation spectra is 6.26 eV; this value is significantly higher than that reported before in literature. In addition, the emission and excitation bands of the F centers have been identified at 445 nm (2.78 eV) and 5.1 eV (243 nm), respectively.

Acknowledgements

The research leading to this result has been supported by the project CALIPSO plus under the Grant Agreement 730872 from the EU Framework Programme for Research and Innovation HORIZON 2020. The work was supported by the Latvian Science Council grant LZP-2018/2-0358. The authors are grateful to K. Chernenko (MAX IV Laboratory, Lund University) for his assistance during beamtime experiments. V.P. also acknowledges Valsts pētījumu programma "Augstas enerģijas fizika un paātrinātāju tehnoloģijas" (Projekta Nr. VPP-IZM-CERN-2020/1-0002).

1. E. L. Belokoneva and N. V. Belov, *Dok. Akad. Nauk SSSR* **260(6)**, 1363 (1981).
2. N. S. Kozlova, A. P. Kozlova, D. A. Spassky, and E. V. Zabelina, *IOP Conf. Series: Materials Science and Engineering* **169**, 012018 (2017).
3. O. A. Buzanov, N. S. Kozlova, A. P. Kozlova, E. V. Zabelina, A. E. Blagov, I. A. Eliovich, A. G. Kulikov, and A. V. Targonskiy, *Jpn. J. Appl. Phys.* **57**, 11UD08 (2018).
4. Sh. Zhang, Y. Zheng, H. Kong, J. Xin, E. Frantz, and Th. R. Shrout, *J. Appl. Phys.* **105**, 114107 (2009).
5. J. Chen, Y. Zheng, H. Kong, and E. Shi, *Appl. Phys. Lett.* **89**, 012901 (2006).
6. R. Lisiecki, W. Ryba-Romanowski, L. Macalik, J. Komar, and M. Berkowski, *Appl. Phys. B* **116**, 183 (2014).
7. H. Kimura, S. Uda, O. Buzanov, X. Huang, and Sh. Koh, *J. Electroceramics* **20**, 73 (2008).
8. Y. Yokota, M. Sato, Y. Futami, K. Tota, T. Yanagida, K. Onodera, and A.Yoshikawa, *J. Cryst. Growth* **352**, 147 (2012).
9. A. Wu, *Cryts. Res. Technol.* **42**, 862 (2007).
10. T. Taishi, T. Hayashi, N. Bamba, Y. Ohno, I. Yonenaga, and W. Hoshikawa, *J. Phys. B* **401**, 437 (2007).
11. O. A. Buzanov, A. V. Naumov, V. V. Nechaev, and S. N. Knyazev, *Proc. 1996 IEEE Int. Freq. Control Symp.* (1996).
12. J. Bohm, R. B. Heimann, M. Hengst, R. Roewer, and J. Schindler, *J. Cryst. Growth* **204**, 128 (1999).
13. F. Chen, F. Yu, Sh. Hou, Y. Liu, Y. Zhou, X. Shi, H. Wang, Zh. Wang, and X. Zhao, *Cryst. Eng. Commun.* **16**, 10286 (2014).
14. B. V. Grinev, M. F. Dubovik, and A. V. Tolmachev, *Optical Complex Oxides Single Crystals*, *Institute of monocrystals*, Institute of Single Crystals, Kharkiv (2002).
15. N. S. Kozlova, O. A. Busanov, E. V. Zabelina, A. P. Kozlova, and M. B. Bykova, *Crystallogr. Rep.* **61**, 275 (2016).
16. X. Tu, Y. Zheng, K. Xiong, Y. Shi, and E. Shi, *J. Cryst. Growth* **401**, 820 (2014).
17. M. Roth, M. Tseitlin, and N. Angert, *Glass Phys. Chem.* **31**, 86 (2005).
18. J. Wang, H. Yu, Y. Wu, and R. Boughton, *Engineering* **1**, 192 (2015).
19. H. Kong, J. Wang, H. Zhang, X. Yin, Sh. Zhang, Y. Liu, X. Cheng, L. Gao, X. Hu, and M. Jiang, *J. Cryst. Growth* **254**, 360 (2003).
20. V. Ivanov, *Opt. Mater.* **79**, 1 (2018).
21. V. Ivanov, A. Stepanov, V. Alenkov, and O. Buzanov, *Opt. Mat. Express* **7**, 3366 (2017).
22. B. Wang, A. Wei, X. Shi, D. Yuan, and H. Qi, *Mat. Lett.* **60**, 2617 (2006).
23. X. Shi, D. Yuan, A. Wei, Z. Wang, and B. Wang, *Mater. Res. Bull.* **41**, 1052 (2006).
24. M. Seifert, *Materials* **13**, 1605 (2020).
25. G. K. Rane, M. Seifert, S. Menzel, T. Gemming, and J. Eckert, *Materials* **9**, 101 (2016).
26. X. Shi, D. Yuan, X. Yin, A. Wei, Sh. Guo, and F. Yu, *Solid. State Commun.* **142**, 173 (2007).
27. O. M. Kugaenko, S. S. Uvarova, S. A. Krylov, B. R. Senatulin, V. S. Petrakov, O. A. Buzanov, V. N. Egorov, and S. A. Sakharov, *Bull. Russ. Acad. Sci.*: *Phys.* **76**, 1258 (2012).
28. B. Mytsyk, Y. Suhak, O. Buryy, N. Demyanyshyn, N. Syvorotka, D. Sugak, and H. Fritze, *IEEE 15th Int. Conf. on Advanced Trends in Radioelectronics, Telecommunications and Computer Engineering (TCSET)*, Lviv, (2020), p. 516.
29. Yu. Suhak, M. Schulz, D. Richter, and H. Fritze, *Solid State Phenom.* **230**, 267 (2015).
30. G. D. Najafpour, *Biochem. Eng. Biotech.*, Elsevier (2015).
31. C. Karunakaran, R. Rajkumar, and K. Bhargava, *Biosensors and Bioelectronics*, Elsevier (2015).
32. M. Brzhezinskaya, A. Irzhak, D. Irzhak, T. W. Kang, O. Kononenko, V. Matveev, G. Panin, and D. Roshchupkin, *Phys. Status Solidi RRL* **10**, 639 (2016).
33. D. A. Spassky, M. G. Brik, N. S. Kozlova, A. P. Kozlova, E. V. Zabelina, O. A. Buzanov, and A. Belsky, *J. Lumin.* **177**, 152 (2016).
34. D. A. Spassky, N. S. Kozlova, A. P. Kozlova, E. V. Zabelina, O. A. Buzanov, M. Buryi, V. Laguta, K. Lebbou, A. Nehari, H. Cabane, M. Dumortier, and V. Nagirnyi, *J. Lumin.* **180**, 95 (2016).
35. O. A. Buzanov, N. S. Kozlova, and N. A. Siminel, *Izvestia VUZov*, *Mater. Elektron. Teh*. **2**, 21 (2012).
36. D. A. Spasskii, N. S. Kozlova, A. P. Kozlova, E. V. Zabelina, and O. A. Buzanov, *Phys. Solid. State* **61**, 307 (2019).
37. A. Reinhardt, A. Zychb, I. Köhlerb, and B. Albert, *J. Lumin.* **218**, 116833 (2020).
38. S. Georgescu, O. Toma, A. M. Chinie, L. Gheorghe, A. Achim, and A. S. Stefan, *Opt. Mater.* **30**, 1007 (2008).
39. Z. Wang, D. Yuan, X. Shi, X. Cheng, D. Xu, M. Lü, and L. Pan, *J. Cryst. Growth* **263**, 246 (2004).
40. Z. Wang, D. Yuan, X. Shi, X. Cheng, D. Xu, M. Lv, L. Pan, and Sh. Guo, *J. Cryst. Growth* **257**, 141 (2003).
41. Z. Wang, Y. Yin, and D. Yuan, *J. Alloys Compd.* **436**, 364 (2007).
42. Z. Wang, D. Yuan, Y. Yin, and G. Su, *Opt. Mater.* **29**, 663 (2007).
43. J. Komar, R. Lisiecki, W. Ryba-Romanowski, and M. Berkowski, *J. Alloys Compd.* **610**, 50 (2014).
44. L. Alyabyeva, V. Burkov, B. Mill, *Opt. Mater.* **43**, 55 (2015).
45. S. Georgescu, O. Toma, A. M. Voiculescu, C. Matei, R. Birjega, and L. Petrescu, *Physica B* **407**, 1124 (2012).

46. M. Itoh, Sh. Takagi, M. Kitaura, M. Fujita, and N. Endo, *J. Lumin.* **122–123**, 205 (2007).
47. Y. Futami, T. Yanagida, Y. Fujimoto, V. Jary, J. Pejchal, Yu. Yokota, M. Kikuchi, M. Nikl, and A. Yoshikawa, *Opt. Mater.* **34**, 1513 (2012).
48. Sh. Kurosawa, M. Kitahara, Y. Yokota, K. Hishinuma, T. Kudo, O. Buzanov, A. Medvedev, V. I. Chani, and A. Yoshikawa, *IEEE Trans. Nucl. Sci.* **61**, 339 (2014).
49. J. Liu, Zh. Wang, K. He, L. Wei, Zh. Zhang, Zh. Wei, H. Yu, H. Zhang, and J. Wang, *Opt. Express* **22**, 5635 (2014).
50. X. Fu, E. G. Villora, Y. Matsushuta, Y. Kitanaka, Y. Noguchi, M. Miyayama, K. Shimamura, and N. Ohashi, *J. Ceram. Soc. Jpn.* **124**, 523 (2016).
51. A. P. Kozlova, V. M. Kasimova, O. A. Buzanov, K. Chernenko, K. Klementiev, and V. Pankratov, *Results Phys.* **16**, 103002 (2020).
52. A. Tuomela, M. Zhang, M. Huttula, S. Sakirzanovas, A. Kareiva, A. I. Popov, A. P. Kozlova, A. S. Aravindh, W. Cao, and V. Pankratov, *J. Alloys Compd.* **826**, 154205 (2020).
53. L. Shirmane, C. Feldmann, and V. Pankratov, *Physica B* **504**, 80 (2017).
54. L. Shirmane and V. Pankratov, *Phys. Status Solidi RRL* **10**, 475 (2016).
55. A. Kuzmin, V. Pankratov, A. Kalinko, A. Kotlov, L. Shirmane, and A. I. Popov, *Fiz. Nizk. Temp.* **42**, 694 (2016) [*Low Temp. Phys.* **42**, 543 (2016)].
56. V. Pankratov, S. Chernov, L. Grigorjeva, T. Chudoba, and W. Lojkowski, *IEEE Trans. Nucl. Sci.* **55**, 1509 (2008).
57. A. Lushchik, Ch. Lushchik, A. I. Popov, K. Schwartz, E. Shablonin, and E. Vasil'chenko, *Nucl. Instrum. Meth. B* **374**, 90 (2016).
58. E. Shablonin, A. I. Popov, A. Lushchik, A. Kotlov, and S. Dolgov, *Physica B* **477**, 133 (2015).
59. A. Kuzmanoski, V. Pankratov, and C. Feldmann, *J. Lumin.* **179**, 555 (2016).
60. A. Tuomela, V. Pankratov, A. Sarakovskis, G. Doke, L. Grinberga, S. Vielhauer, and M. Huttula, *J. Lumin.* **179**, 16 (2016).
61. V. Pankratov, M. Kirm, and H. von Seggern, *Phys. Status Solidi C* **2**, 371 (2005).
62. A. Lushchik, Ch. Lushchik, E. Vasil'chenko, and A. I. Popov, *Fiz. Nizk. Temper.* **44**, 357 (2018) [*Low Temp. Phys.* **44**, 269 (2018)].
63. V. Pankratov, A. I. Popov, L. Shirmane, A. Kotlov, G. A. Bizarri, A. Burger, P. Bhattacharya, E. Tupitsyn, E. Rowe, V. M. Buliga, R. T. Williams, *Radiat. Meas.* **56**, 13 (2013).
64. A. Shalaev, R. Shendrik, A. Rusakov, A. Bogdanov, V. Pankratov, K. Chernenko, A. Myasnikova, *Nucl. Instrum. Meth. B* **467**, 17 (2020).
65. P. V. Savchyn, V. V. Vistovskyy, A. S. Pushak, A. S. Voloshinovskii, A. V. Gektin, V. Pankratov, and A. I. Popov, *Nucl. Instrum. Meth. B* **274**, 78 (2012).
66. M. Dendebera, Y. Chornodolskyy, R. Gamernyk, O. Antonyak, I. Pashuk, S. Myagkota, I. Gnilitskyi, V. Pankratov, V. Mikhailik, M. Grinberg, and A. Voloshinovskii, *J. Lumin.* **225**, 117346 (2020).
67. L. Grigorjeva, D. Millers, J. Grabis, C. Monty, A. Kalinko, K. Smits, V. Pankratov, and W. Lojkowski, *IEEE Trans. Nucl. Sci.* **55**, 1551 (2008).
68. V. Pankratov, V. Osinniy, A. Nylandsted Larsen, and B. Bech Nielsen, *Phys. Rev. B* **83**, 045308 (2011).
69. V. Pankratov, J. Hoszowska, J.-Cl. Dousse, M. Huttula, A. Kis, D. Krasnozhon, M. Zhang, and W. Cao, *J. Phys. Condens. Matter* **28**, 015301 (2016).
70. V. Pankratov and A. Kotlov, *Nucl. Instrum. Meth. B* **474**, 35 (2020).
71. V. Pankratov, R. Pärna, M. Kirm, V. Nagirnyi, E. Nõmmiste, S. Omelkov, S. Vielhauer, K. Chernenko, L. Leisberg, P. Turunen, A. Kivimäki, E. Kukk, M. Valden, and M. Huttula, *Radiat. Meas.* **121**, 91 (2019).
72. R. Pärna, R. Sankari, E. Kukk, E. Nõmmiste, M. Valden, M. Lastusaari, K. Kooser, K. Kokko, M. Hirsimäki, S. Urpelainen, P. Turunen, A. Kivimäki, V. Pankratov, L. Reisberg, L. F. Hennies, H. Tarawneh, R. Nyholm, and M. Huttula, *Nucl. Instrum. Meth. A* **859**, 83 (2017).
73. *Phosphor Handbook*, S. Shionoya, W. M. Yen, and H. Yamamoto (eds.), CRC press (2007).
74. L. Grigorjeva, D. Millers, S. Chernov, M. Nikl, Y. Usuki, and V. Pankratov, *Nucl. Instrum. Meth. B* **166-167**, 329 (2000).
75. D. Millers, L. Grigorjeva, S. Chernov, A. Popov, P. Lecoq, and E. Auffray, *Phys. Status Solidi B* **203**, 585 (1997).
76. A. Kuzmanoski, V. Pankratov, and C. Feldmann, *Solid State Sci.* **41**, 56 (2015).
77. L. Grigorjeva, V. Pankratov, D. Millers, G. Corradi, and K. Polgar, *Integr. Ferroelectr.* **35**, 137 (2001).
78. L. Grigorjeva, D. Millers, V. Pankratov, R. T. Williams, R. I. Eglitis, E. A. Kotomin, and G. Borstel, *Solid State Commun.* **129**, 691 (2004).
79. L. Grigorjeva, D. Millers, A. I. Popov, E. A. Kotomin, and E. S. Polzik, *J. Lumin.* **72–74**, 672 (1997).
80. A. Popov and E. Balanzat, *Nucl. Instrum. Meth. B* **166–167**, 305 (2000).
81. D. Millers, V. Pankratov, L. Grigorjeva, S. Kapphan, and V. Trepakov, *Radiat. Eff. Defects Solids* **157**, 589 (2002).
82. A. I. Popov, E. A. Kotomin, and J. Maier, *Nucl. Instrum. Meth. B* **268**, 3084 (2010).

Низькотемпературна люмінесценція монокристалів катангасита при збудженні синхротронним вакуумним ультрафіолетовим випромінюванням.

A. P. Kozlova, O. A. Buzanov, V. Pankratova, V. Pankratov

Люмінесцентні властивості монокристалів $Ca_3TaGa_3Si_2O_{14}$ (CTGS, катангасит) досліджено методом вакуумної ультрафіолетової спектроскопії з використанням синхротронної установки MAX IV з енергією випромінювання 1,5 ГеВ. Виявлено дві смуги випромінювання при 320 нм (3,87 еВ) та 445 нм (2,78 еВ). При дослідженні збуджень у спектральному ВУФ діапазоні смуга випромінювання при 320 нм була інтерпретована як смуга випромінювання автолокалізованих екситонів у монокристалі CTGS. Обговорено її атомну структуру. Крім того, запропоновано, що емісія при 445 нм (2,78 еВ) у CTGS обумовлена *F* центрами, для яких спостерігається смуга збудження (поглинання), яка добре розрізняється при 5,1 еВ (243 нм).

Ключові слова: катангасит, лангасит, лангатат, ВУФ люмінесцентна спектроскопія, синхротронне випромінювання.